Universal Aging Mechanism for Static and Sliding Friction of Metallic Nanoparticles

Michael Feldmann,[1] Dirk Dietzel,[1,*] Antoni Tekiel,[2] Jessica Topple,[2] Peter Grütter,[2] and André Schirmeisen[1,†]
[1]Institute of Applied Physics, Justus-Liebig-Universität Giessen, 35392 Giessen, Germany
[2]Department of Physics, McGill University, Montreal, Quebec H3A 2T8, Canada
(Received 29 February 2016; revised manuscript received 10 May 2016; published 8 July 2016)

The term "contact aging" refers to the temporal evolution of the interface between a slider and a substrate usually resulting in increasing friction with time. Current phenomenological models for multiasperity contacts anticipate that such aging is not only the driving force behind the transition from static to sliding friction, but at the same time influences the general dynamics of the sliding friction process. To correlate static and sliding friction on the nanoscale, we show experimental evidence of stick-slip friction for nanoparticles sliding on graphite over a wide dynamic range. We can assign defined periods of aging to the stick phases of the particles, which agree with simulations explicitly including contact aging. Additional slide-hold-slide experiments for the same system allow linking the sliding friction results to static friction measurements, where both friction mechanisms can be universally described by a common aging formalism.

DOI: 10.1103/PhysRevLett.117.025502

The force needed to initiate sliding of an object is usually higher than the force needed to sustain its motion, which is termed static and sliding friction [1,2]. Early investigators have attributed this difference to the inevitable surface roughness between interfaces and the number of true contact points where their asperities meet [3]. Upon external shear these asperities exhibit a transient creeplike motion leading to static and kinetic friction [4–7]. It is commonly believed that the threshold for sliding initiation is higher than for sustaining sliding, which is caused by aging phenomena, i.e., an increase of asperity interaction with time [8–12]. Friction of such rough interfaces can be well described in the framework of rate and state theories [13,14], where contact aging is assigned to the not further specified state variable Θ. This parameter is usually interpreted as the number (or overall area) of contact points, but may also be related to other interface processes [15]. These models anticipate that aging is not only the driving force behind the transition from static to sliding friction, but at the same time influences the general dynamics of the sliding friction process.

However, the atomistic interpretation of contact aging remains difficult, especially since nanoscale contact aging has been studied only in a few experiments up to now. Studied examples range from atomic stick slip on graphite [16], aging of diamond-silicate contacts [17], to nanoparticle friction [18,19]. One unresolved question is whether contact aging is solely responsible for the static friction threshold. Also, it remains unknown how to connect contact aging to individual stick-slip events, which are inevitably present during sliding.

Our goal was to analyze a model friction system, which shows stick-slip behavior and exhibits aging without wear or other irreversible interface changes over time. For this we performed experiments of sliding metallic nanoparticles on a flat surface in ultrahigh vacuum (UHV) conditions. Stick-slip motion of the particles during sliding is clearly resolved for a large variation of sliding speeds and our analysis of a large set of individual stick-slip events shows that the slip force increases systematically with the stick-time during continuous sliding. This is complemented by slide-hold-slide measurements [17] of the static friction force. We show that static and sliding friction can essentially be described by the same universal law, which is based on thermally activated contact breaking combined with logarithmic contact aging. This allows us to close the gap between static and sliding friction over 5 orders of magnitude in time scale.

All nanomanipulation experiments have been performed using antimony nanoparticles prepared under UHV conditions by thermal evaporation onto freshly cleaved HOPG [Fig. 1(a)]. The crucible of a conventional Knudsen cell containing antimony was heated up to 450 °C and the evaporation time was about 7 min at a rate of approximately 6.5 Å/ min. Directly afterwards, the sample was transferred to the UHV atomic force microscope (AFM; type: JEOL JSPM-4500A) without breaking the vacuum. All measurements were done at room temperature and the average sliding friction values were in quantitative agreement with values of superlubric sliding found before [20], thus indicating an atomically clean interface [21]. The nanomanipulation measurements were performed using the "tip on side" mode, where the AFM tip was placed directly beside the nanoparticle [20–22]. The manipulation sequences were live monitored by an integrated scanning electron microscope, which induced no apparent changes in friction. The adhesion between tip and nanoparticle was typically strong enough to enable pushing as well as pulling of the particle [Fig. 1(b)]. This allows measuring the lateral force signals

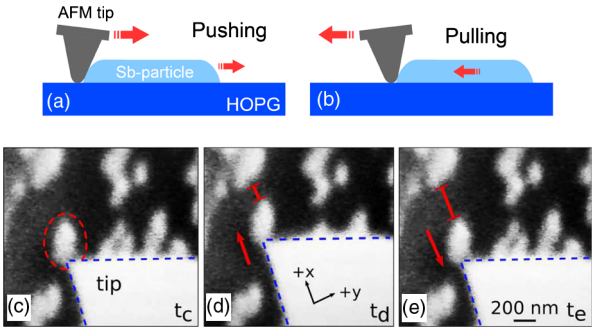

FIG. 1. (a)–(b) Schematic diagrams illustrating the concept of nanoparticle manipulation based on the tip-on-side approach. Because of adhesion between particle and substrate, both pushing (a) and pulling (b) is possible. (c)–(e) Three frames extracted from scanning electron microscopy live video captured during the manipulation of an Sb nanoparticle ($A_{\mathrm{contact}} = 59000\ \mathrm{nm}^2$) on HOPG. The three frames in chronological order ($t_c < t_d < t_e$) illustrate the pushing and the pulling process.

in two opposite sliding directions to obtain complete friction loops (friction between tip and HOPG was below 0.4 nN at all times and was thus negligible). In order to monitor the stick-slip movement of the nanoparticles an AD converter with high data acquisition rate was used in parallel to the main AFM scan control electronics [23]. Here we present measurements for three different nanoparticles with sliding velocities ranging from 0.1 nm/s up to 1 μm/s.

Figure 2(a) shows a typical friction loop for the nanoparticle in Fig. 1, where discontinuous stick-slip friction is found. The lateral force build-up between two slip events is linear until the maximum lateral force $F_{L,\mathrm{max}}$ is reached [Fig. 2(b)] after a tip base movement of $\Delta x_{\mathrm{stick}}$. This confirms that the contact between particle and substrate is firm and does not show any relaxation prior to the slip itself. At the same time, we observe a very steep decline in lateral force down to $F_{L,\mathrm{min}}$ once the slip is initiated, compatible with a rigid particle picture. Often, oscillations can be observed after a slip event, showing a high frequency ringdown ($f_{\mathrm{ringdown}} \approx 1.5$–$3$ kHz) [23].

An automated detection routine was used to identify all minima $F_{L,\mathrm{min}}$ and maxima $F_{L,\mathrm{max}}$ of the lateral forces related to beginning and end of a stick phase. From this the corresponding stick $\Delta x_{\mathrm{stick}}$ as well as slip distances Δx_{slip} were calculated [Fig. 2(b)]. For all sliding velocities stick-slip was observed with both $F_{L,\mathrm{max}}$ and $F_{L,\mathrm{min}}$ showing a statistical distribution as illustrated in Figs. 2(c) and 2(d) for $v_{\mathrm{sliding}} = 20$ nm/s. The slip distances Δx_{slip} varied from 0.3 to 5 nm. Slip lengths smaller than the lattice constant of HOPG have never been observed.

In conventional friction force microscopy [27,28] crystalline HOPG substrates usually produce perfectly regular stick-slip patterns with a lattice periodicity of 0.24 nm. Here, in contrast, we find irregular stick slip with Δx_{slip} in the nm range, which is plausible given the complex amorphous-crystalline interface structure between particle and substrate. The effective lateral spring constant (slope of

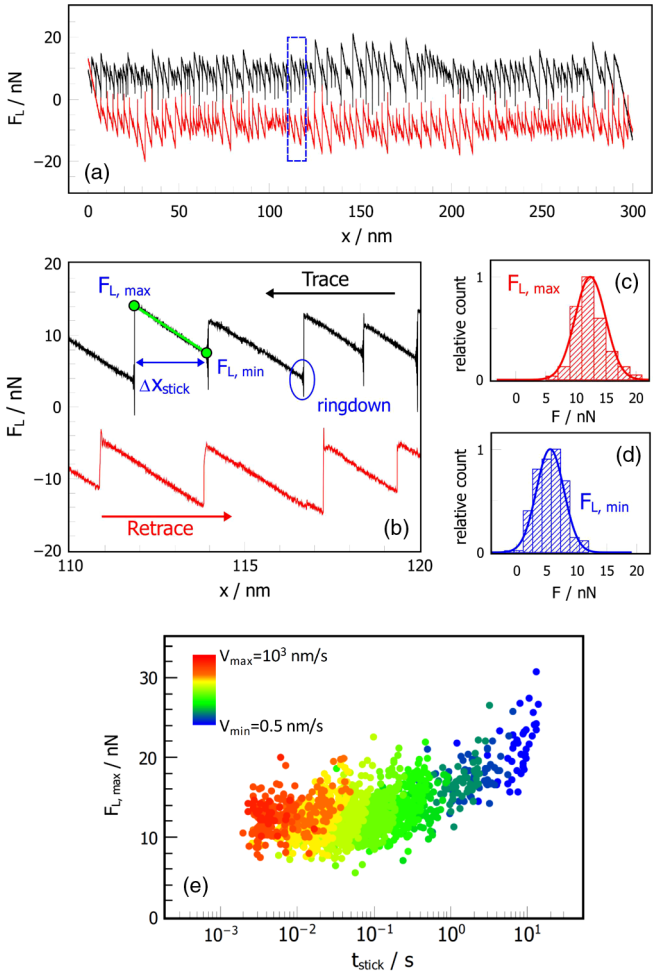

FIG. 2. (a) Friction loop during pulling and pushing of an Sb nanoparticle on HOPG with a contact area of $A = 59000\ \mathrm{nm}^2$ at a sliding velocity of $v = 20$ nm/s showing stick-slip motion. (b) Close-up view of a number of stick-slip cycles from (a). A pair of $F_{L,\mathrm{max}}$ and $F_{L,\mathrm{min}}$ is indicated by the green spheres, with a linear force buildup in between. Often lateral force minima after the slip show friction spikes which are high frequency dissipative ringdowns. (c),(d) Typical distribution of $F_{L,\mathrm{max}}$ and $F_{L,\mathrm{min}}$ for a velocity of 20 nm/s. (e) Slip inducing forces $F_{L,\mathrm{max}}$ of the particle measured for 11 velocities between 0.5 nm/s and 1 μm/s plotted versus the corresponding stick time $t_{\mathrm{stick}} = x_{\mathrm{stick}}/v$.

the friction curve in the stick phase) was around 3 N/m. With a nominal lateral spring constant of the cantilever of 15 N/m this leads to an effective tip-particle spring constant of around 4 N/m.

The well-defined, albeit irregular, stick-slip movement of the nanoparticles now opens up a straightforward route to characterize contact aging effects during particle sliding. Here we can directly associate each lateral force peak with its preceding rest time. This is demonstrated in Fig. 2(e): For each sliding velocity v, all values $F_{L,\mathrm{max}}$, $F_{L,\mathrm{min}}$, and $\Delta x_{\mathrm{stick}}$ have been determined and the corresponding stick times were calculated by $t_{\mathrm{stick}} = \Delta x_{\mathrm{stick}} v_{\mathrm{tip}}^{-1}$ resulting in ≈1500 data points altogether. Sliding velocities were varied over more than 3 orders of magnitude from 0.5 to

1000 nm/s, resulting in a similar large range of statistically distributed stick times.

In Fig. 2(e) we plot the slip inducing force $F_{L,\max}$ vs the hold time t_{stick}. Data points obtained for the different sliding velocities (color coded) form overlapping "clouds," which spread both in t_{stick} and $F_{\max}$. Despite this scatter Fig. 2(e) shows a systematic increase of $F_{L,\max}$ as a function of the stick time for $t_{\text{stick}} > 100$ ms. In this case, $F_{L,\max}$ changes by about 100%, demonstrating that contact aging significantly influences the friction of metallic nanoparticles.

In order to establish a connection between the experimental data and the temporal aging process, we have performed simulations of the contact breaking process, including thermal activation [29–32]. We model the contact rupture as thermally assisted escape from a bound state over an activation barrier ΔE_{detach}, which is force dependent and diminishes as the applied pulling force increases [33,34]. The sliding object is initially trapped in a local energy minimum, where a critical force F_{critical} is required to break the contact and initiate the slip [cf. schematic energy diagram in Fig. 3(a)]. Sang *et al.* have found that the energy barrier decreases with increasing lateral force according to $\Delta E_{\text{detach}} \propto (F_{\text{critical}} - F_L)^{3/2}$. We assume that the critical force is proportional to the particle substrate energy barrier, which changes as a function of particle rest time (see Supplemental Material for further details [23]).

First we simulated thermally activated slip with a constant energy barrier between particle and substrate, i.e., in the absence of contact aging [Fig. 3(c)]. Here, data pairs $F_{L,\max}$ vs t_{stick} fall onto separate curves representing the different scan velocities. Obviously, without contact aging, this does not reproduce the experimental trend in Fig. 2(e). Instead, increasing hold times, corresponding to decreasing sliding velocities, results in decreasing $F_{L,\max}$, a direct consequence of thermal activation.

In the second step we implemented contact aging by assuming an exponential dependence of the energy barrier on rest time [18]:

$$\Delta E(t) = \Delta E_0 + \Delta E_{\text{aging}}[1 - e^{-(t/\tau)^{\alpha}}]. \qquad (1)$$

Here, ΔE_0 represents the initial energy barrier directly after attachment, ΔE_{aging} the maximum amount of aging, whose time scale is described by τ. The above equation results in a logarithmlike increase of the contact stiffness on a time scale of τ. The exponential stretch factor α takes into account that the effective energy barrier results from multiple individual bonds with a broad statistical distribution as expected for an amorphous interface [18,35].

Now the critical force, and thus ΔE_{detach}, become time dependent. A statistical evaluation of the slip inducing force shows the fingerprint of contact aging [Fig. 3(d)]: The force $F_{L,\max}$ increases with rest time t_{stick}, in agreement with the experiments.

However, the simulated data points fall onto narrow lines, while the experimental data are of cloudlike shape.

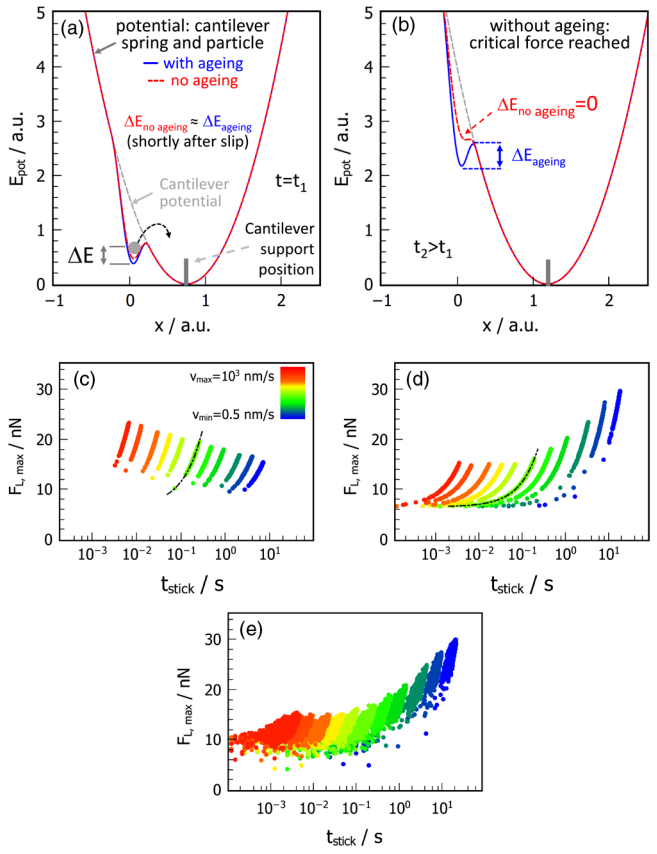

FIG. 3. (a) Schematic energy diagram of a nanoparticle on a flat surface in contact with a cantilever spring at $t = t_1$. (b) Energy diagram for $t_2 > t_1$ when the cantilever support has moved by $\Delta x = v(t_2 - t_1)$. Without aging the energy barrier is zero, but with aging an effective residual energy barrier of ΔE_{aging} remains. (c) Simulation of thermally activated slip inducing forces as a function of hold time without aging, where each stick period started at $F_{L,\min} = 6.5$ nN. (d) Same simulation as in (c) but now including aging. The dashed lines in (c) and (d) indicate the force values corresponding to $F_L = F_{L,\min} + t_{\text{stick}} vk$ ($v = 20$ nm/s). (e) Same simulation as in (d), i.e., including thermal activation and contact aging, but now assuming a Gaussian distribution of $F_{L,\min}$. (Please note that an increased energy barrier ΔE_0 was used in (c) to match the range of hold times of (d) and (e).

The reason is that in Figs. 3(c) and 3(d) after each slip the lateral force relaxes down to a uniform value $F_{L,\min}$. Consequently, only lateral forces described by $F_L = F_{L,\min} + t_{\text{stick}} vk$ are possible (with effective spring constant k), and each line in Figs. 3(c) and 3(d) corresponds to a different sliding velocity v. But clearly Fig. 2(d) shows that the cantilever relaxation is not uniform. Instead, $F_{L,\min}$ is well described by a Gaussian distribution independent of v, where any force values $|F_{L,\min} - F_{L,\min,\text{center}}| > 4$ nN are discarded. Now, similar hold times can be related to different $F_{L,\max}$ despite the linear cantilever loading curve. In Fig. 3(e) we show our simulation, including contact aging as well as the statistical $F_{L,\min}$ distribution. The general curve progression and the distribution of data points show excellent agreement between experiment and simulation.

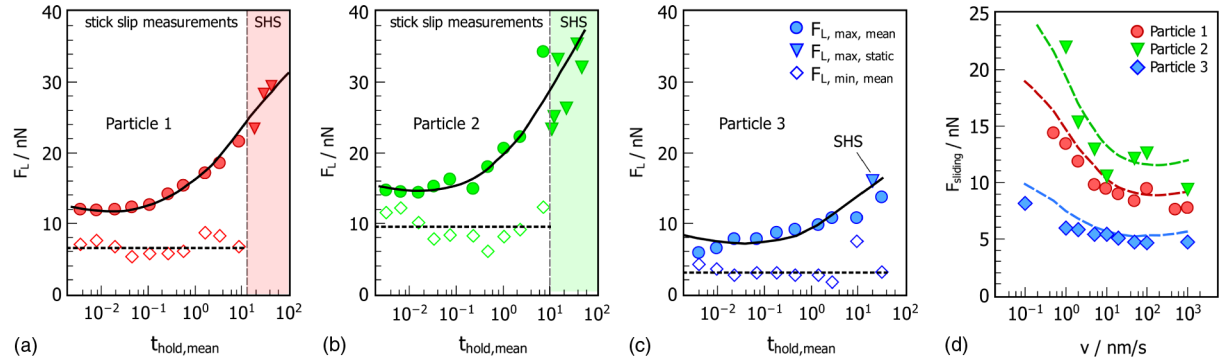

FIG. 4. (a)–(c) Averaged maximum lateral forces $F_{L,\mathrm{max,ave}}$ (spheres) and minimum lateral forces $F_{L,\mathrm{min,ave}}$ (diamonds) during nanoparticle stick-slip motion for 0.1 nm/s < v < 1 μm/s plotted vs the average hold time for three different particles with contact areas of 59 000 (a), 31 000 (b), and 18000 nm^2 (c). Static friction peaks are shown as triangles. Numerical simulations have been fitted to the maximum lateral forces (solid black lines, see text and Ref. [23] for parameters). Dashed lines indicate average minimum lateral force $F_{L,\mathrm{min}}$ values used in the simulations. (d) Velocity dependence of the mean kinetic friction measured for same the three nanoparticles as shown in (a)–(c) together with theoretical simulations (dashed lines) based on the parameters used in (a)–(c).

For better comparison we have calculated the average lateral forces $F_{L,\mathrm{max,ave}}$ and $F_{L,\mathrm{min,ave}}$ as a function of the average hold time $t_{\mathrm{stick,ave}}$. The results are shown for three different nanoparticles in Fig. 4. Please note that in contrast to $F_{L,\mathrm{max,ave}}$, the $F_{L,\mathrm{min,ave}}$ data show only minor variations with v and t_{stick}, in retrospect justifying our approach of assuming a constant distribution of $F_{L,\mathrm{min}}$.

The experimental data can be fitted very well by the average lateral force values derived from the simulations using $\tau_1 = 8.5^{+7}_{-3}$, $\tau_2 = 9^{+6}_{-3}$, and $\tau_3 = 8^{+5}_{-3}$ sec for the three nanoparticles with contact areas of 59 000 (a), 31 000 (b), and 18000 nm^2 (c). The stretch factors were $\alpha_1 = 0.35^{+0.1}_{-0.05}$, $\alpha_2 = 0.4^{+0.1}_{-0.05}$, and $\alpha_3 = 0.3^{+0.05}_{-0.05}$, respectively. There seems to be no systematic variation of the aging parameters with contact area in the investigated size regime.

In our model we treat each slip event as an independent process. In order to verify whether successive stick-slip motion is based on the same mechanism as static friction measurements, we additionally used the slide-hold-slide protocols introduced in Ref. [17]. After the nanoparticles were pushed by the AFM tip, the cantilever movement was stopped for a defined time period ($t_{\mathrm{rest}} \gtrsim 10$ s). Then particle pushing was reinitiated, resulting in distinct static friction peaks [20,36] (triangles in Fig. 4). The static friction data fits well to a continuous extrapolation of $F_{L,\mathrm{max}}$ from stick-slip sliding, strongly suggesting that the aging mechanism during stick-slip movement is equivalent to aging with complete suspension of movement. Thus, the different shear and dynamic conditions do not significantly influence the aging process.

Usually, well defined stick-slip behavior is experimentally not directly accessible, and instead the velocity dependence is analyzed [18,31,32,37–40]. Thus, we have calculated sliding friction as a function of velocity both from our experiments and from simulations in Fig. 4(d) [same parameters as in 4(a)–4(c)]. We find good agreement between experiment and theory, with a clear trend of "velocity weakening" in both. This means that modeling sliding friction based on stick-slip movement with simultaneous contact aging is a valid approach.

At this point the question about the physical origin for the observed contact aging of the nanoparticle-graphite interface still remains. Molecular dynamics simulations for Au and Ag nanoparticles on HOPG have indicated atomic relaxations at the particle-substrate interface that are time dependent [41]. These relaxations resulted in the formation of commensurate patches at the nanoparticle-substrate interface. This aging process is illustrated in Fig. 5 for the case of amorphous antimony nanoparticles on HOPG. Amorphous Sb on HOPG is superlubric with very small friction values [20,21]. Recently, Kawai *et al.* demonstrated how sensitively friction of a graphene nanoribbon is influenced by small changes in local commensurability related to surface reconstruction of the Au(111) substrate [42]. Therefore, the formation of even very small commensurate patches will constitute a significant change in the overall shear stress and substantial aging with time is conceivable. The complex reorientation processes required to reach commensurate configuration may explain the long aging time scales observed here, but still need to be

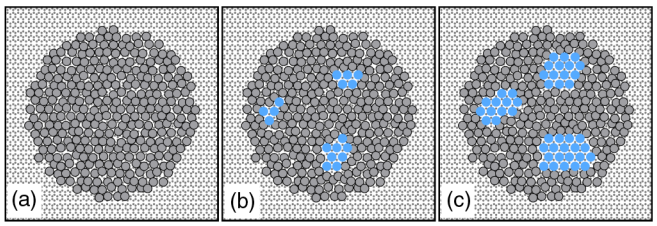

FIG. 5. Schematic concept for nanoparticle contact aging: (a) The amorphous nanoparticle is initially resting on the substrate in fully incommensurate configuration. (b) Relaxation processes on the atomic level will lead to the nucleation of commensurate subareas (blue spheres) at the interface. (c) With time these subareas will grow.

corroborated by specific simulations for the Sb/HOPG system.

Our results essentially show that contact aging exists for Sb nanoparticles by correlating stick times to the slip inducing lateral force values. Despite conceptual differences, the aging process during quasicontinuous stick-slip movement and aging during complete halt of movement appear to be equivalent; i.e., the different shear conditions at the interface seem to be of minor relevance. Our simulations show that for this system aging can be universally described by a simple exponential aging law. The limited number of particles investigated does not yet allow us to quantify the influence of particle size on ageing. Especially the methodology of high resolution stick-slip measurements opens further perspectives to understand interface processes of extended nanocontacts. In this context, analyzing the lateral force buildup during pushing seems particularly promising. In our case, this buildup was completely linear, in agreement with the assumption of rigid particles. However, pre-slip relaxations might be expected for nonrigid interfaces or for contaminated interfaces [21], where theory predicts relaxations of the molecules between two incommensurate surfaces in motion [43,44].

Financial support was provided by the German Research Foundation (Project DI917/5-1) and in part by COST Action MP1303 and LaMa of JLU Giessen. P. G. acknowledges support by NSERC and CFI.

*dirk.dietzel@ap.physik.uni-giessen.de
†schirmeisen@uni-giessen.de

[1] B. N. J. Persson, O. Albohr, F. Mancosu, V. Peveri, V. N. Samoilov, and I. M. Sivebaek, Wear **254**, 835 (2003).
[2] B. N. J. Persson, *Sliding Friction* (Springer-Verlag, Berlin, Heidelberg, 2000).
[3] F. P. Bowden and D. Tabor, Proc. R. Soc. A **169**, 391 (1939).
[4] Z. Yang, H. P. Zhang, and M. Marder, Proc. Natl. Acad. Sci. U.S.A. **105**, 13264 (2008).
[5] P. Berthoud and T. Baumberger, Europhys. Lett. **41**, 617 (1998).
[6] A. Goedecke, *Transient Effects in Friction—Fractal Asperity Creep* (Springer Science and Business Media, New York, 2014).
[7] F. Heslot, T. Baumberger, B. Perrin, B. Caroli, and C. Caroli, Phys. Rev. E **49**, 4973 (1994).
[8] J. H. Dieterich, J. Geophys. Res. **84**, 2161 (1979).
[9] T. Baumberger and C. Caroli, Adv. Phys. **55**, 279 (2006).
[10] L. Bureau, T. Baumberger, and C. Caroli, Eur. Phys. J. E **8**, 331 (2002).
[11] O. Ben-David, S. M. Rubinstein, and J. Fineberg, Nature (London) **463**, 76 (2010).
[12] C. H. Scholz, Nature (London) **391**, 37 (1998).
[13] J. R. Rice and A. L. Ruina, J. Appl. Mech. **50**, 343 (1983).
[14] A. L. Ruina, J. Geophys. Res. **88**, 10359 (1983).
[15] Z. Liu, J. Yang, F. Grey, J. Z. Liu, Y. Liu, Y. Wang, Y. Yang, Y. Cheng, and Q. Zheng, Phys. Rev. Lett. **108**, 205503 (2012).
[16] M. Evstigneev, A. Schirmeisen, L. Jansen, H. Fuchs, and P. Reimann, J. Phys. Condens. Matter **20**, 354001 (2008).
[17] Q. Li, T. E. Tullis, D. Goldsby, and R. W. Carpick, Nature (London) **480**, 233 (2011).
[18] M. Feldmann, D. Dietzel, H. Fuchs, and A. Schirmeisen, Phys. Rev. Lett. **112**, 155503 (2014).
[19] D. Dietzel, M. Feldmann, H. Fuchs, U. D. Schwarz, and A. Schirmeisen, Appl. Phys. Lett. **95**, 053104 (2009).
[20] D. Dietzel, M. Feldmann, U. D. Schwarz, H. Fuchs, and A. Schirmeisen, Phys. Rev. Lett. **111**, 235502 (2013).
[21] D. Dietzel, C. Ritter, T. Mönninghoff, H. Fuchs, A. Schirmeisen, and U. D. Schwarz, Phys. Rev. Lett. **101**, 125505 (2008).
[22] D. Dietzel, U. D. Schwarz, and A. Schirmeisen, Friction **2**, 114 (2014).
[23] See Supplemental Material at http://link.aps.org/supplemental/10.1103/PhysRevLett.117.025502 for further details on the experiments and the theory, which includes Refs. [24–26].
[24] A. Socoliuc, R. Bennewitz, E. Gnecco, and E. Meyer, Phys. Rev. Lett. **92**, 134301 (2004).
[25] Y. Liu and I. Szlufarska, Phys. Rev. Lett. **109**, 186102 (2012).
[26] J. Klein, Phys. Rev. Lett. **98**, 056101 (2007).
[27] C. M. Mate, G. M. McClelland, R. Erlandsson, and S. Chiang, Phys. Rev. Lett. **59**, 1942 (1987).
[28] A. Schirmeisen, L. Jansen, and H. Fuchs, Phys. Rev. B **71**, 245403 (2005).
[29] I. Barel, M. Urbakh, L. Jansen, and A. Schirmeisen, Phys. Rev. Lett. **104**, 066104 (2010).
[30] O. Dudko, A. Filippov, J. Klafter, and M. Urbakh, Chem. Phys. Lett. **352**, 499 (2002).
[31] E. Gnecco, R. Bennewitz, T. Gyalog, C. Loppacher, M. Bammerlin, E. Meyer, and H. J. Güntherodt, Phys. Rev. Lett. **84**, 1172 (2000).
[32] Y. Sang, M. Dubé, and M. Grant, Phys. Rev. Lett. **87**, 174301 (2001).
[33] A. E. Filippov, J. Klafter, and M. Urbakh, Phys. Rev. Lett. **92**, 135503 (2004).
[34] M. J. Brukman, G. Gao, R. J. Nemanich, and J. A. Harrison, J. Phys. Chem. C **112**, 9358 (2008).
[35] D. C. Johnston, Phys. Rev. B **74**, 184430 (2006).
[36] R. Lüthi, E. Meyer, H. Haefke, L. Howald, W. Gutmannsbauer, and H.-J. Güntherodt, Science **266**, 1979 (1994).
[37] O. Zwörner, H. Hölscher, U. D. Schwarz, and R. Wiesendanger, Appl. Phys. A **66**, S263 (1998).
[38] E. Riedo, E. Gnecco, R. Bennewitz, E. Meyer, and H. Brune, Phys. Rev. Lett. **91**, 084502 (2003).
[39] I. Barel, M. Urbakh, L. Jansen, and A. Schirmeisen, Phys. Rev. B **84**, 115417 (2011).
[40] A. Schirmeisen, L. Jansen, H. Hölscher, and H. Fuchs, Appl. Phys. Lett. **88**, 123108 (2006).
[41] A. V. Khomenko, N. V. Prodanov, and B. N. J. Persson, Condens. Matter Phys. **16**, 33401 (2013).
[42] S. Kawai, A. Benassi, E. Gnecco, H. Sode, R. Pawlak, X. Feng, K. Mullen, D. Passerone, C. A. Pignedoli, P. Ruffieux, R. Fasel, and E. Meyer, Science **351**, 957 (2016).
[43] J. Brndiar, R. Turansk, D. Dietzel, A. Schirmeisen, and I. Stich, Nanotechnology **22**, 085704 (2011).
[44] M. H. Müser, L. Wenning, and M. O. Robbins, Phys. Rev. Lett. **86**, 1295 (2001).